Mono- and Trivalent Ions around DNA: A Small-Angle Scattering Study of Competition and Interactions

Kurt Andresen, Xiangyun Qiu, Suzette A. Pabit, Jessica S. Lamb, Hye Yoon Park, Lisa W. Kwok, and Lois Pollack
School of Applied and Engineering Physics, Cornell University, Ithaca, New York

ABSTRACT The presence of small numbers of multivalent ions in DNA-containing solutions results in strong attractive forces between DNA strands. Despite the biological importance of this interaction, e.g., DNA condensation, its physical origin remains elusive. We carried out a series of experiments to probe interactions between short DNA strands as small numbers of trivalent ions are included in a solution containing DNA and monovalent ions. Using resonant (anomalous) and nonresonant small angle x-ray scattering, we coordinated measurements of the number and distribution of each ion species around the DNA with the onset of attractive forces between DNA strands. DNA-DNA interactions occur as the number of trivalent ions increases. Surprisingly good agreement is found between data and size-corrected numerical Poisson-Boltzmann predictions of ion competition for non- and weakly interacting DNAs. We also obtained an estimate for the minimum number of trivalent ions needed to initiate DNA-DNA attraction.

INTRODUCTION

Despite extensive studies of electrostatic interactions between DNAs, the physical origin of attraction between highly-negatively charged DNA molecules remains an open question. Much of the DNA's behavior arises from its interactions with other charged bodies, notably the charge-compensating ions that surround each strand. A theoretical description of this so-called ion atmosphere has been relatively well established for lower valence ions (1–3); however, a description of the nonspecific binding of ions of +3 or greater valence remains unresolved (4–9). A thorough physical understanding of the role of multivalent ions in DNA interactions is necessary because important biological processes are mediated by polycations, notably DNA condensation (10).

The Poisson-Boltzmann (PB) equation has been used extensively to quantify interactions between charged particles in solution (11). The full power of this method for describing the counterion atmosphere around DNA was realized after the emergence of Manning's counterion condensation theory (1). Solutions to the PB equation improved on Manning's theory by providing detailed information about the distribution of these ions. These solutions yield realistic descriptions of ion atmospheres around DNA and other highly charged molecules (12–15).

The Poisson-Boltzmann equation is known to describe monovalent ion atmospheres quite accurately, and divalent ion atmospheres to a lesser extent (16); however, it is expected to fail when ions of valence ≥ 3 are present (17). The condensation of DNA and its subsequent redissolution upon multivalent ion titration, also referred to as reentrant condensation, is the most often cited evidence for the predicted shortcomings of this approach (5,18–20).

The most prominent theories suggest that the breakdown results from correlations between discrete counterions along the axial direction of the DNA. Such interactions are not accounted for in the mean field/continuum PB formalism. The addition of ionic correlations can explain the physical origin of DNA condensation; however, there is disagreement about the exact mechanism of attraction. One theory predicts the formation of a self-avoiding Wigner-type lattice that leads to an increase in multivalent ion concentrations; enhanced compensation of the DNA charge by counterions occurs until the charge is reversed (5). Another prominent theory predicts counterion density waves, fluctuating areas of high and low charge density along the polyelectrolyte axis, a behavior that has been observed in systems other than DNA (21). A third theory invokes the formation of salt bridges to explain the condensation (7). Despite relatively diverse mechanisms, all of these theories predict stronger binding of multivalent ions to DNA than predicted by the Poisson-Boltzmann equation. Furthermore, although PB does not accurately describe the system at high multivalent counterion concentrations, its validity has not been tested for concentrations below those critical for condensation.

Here, we report measurements targeting the initiation of trivalent ion-mediated attractive forces between DNA strands in a dilute solution. Our goal is to provide experimental data for comparison with theory, before and at the onset of attraction. Measurements of multivalent ions in competition with monovalent ions is an effective tool for testing the accuracy of such theoretical predictions. In an effort to pinpoint the breakdown of PB, we performed experiments at ion concentrations ranging from those well below the threshold multivalent concentration for DNA condensation up to con-

Submitted October 2, 2007, and accepted for publication February 12, 2008.

Address reprint requests to Lois Pollack, Tel.: 607-255-8695; E-mail: lp26@cornell.edu.

Editor: David P. Millar.

© 2008 by the Biophysical Society

0006-3495/08/07/287/09 $2.00

doi: 10.1529/biophysj.107.123174

centrations where condensation was observed. We started with DNA in a solution containing only monovalent ions. Measurements of the ion atmosphere continued as the trivalent ions were added, essentially one-by-one, while their effect on the DNA was monitored. Although the competition between monovalent and multivalent salts has been studied previously by monitoring changes at the onset of DNA condensation (6,19,20,22–24), few direct measurements of monovalent-trivalent binding competition have been reported (25,26).

The anomalous small-angle x-ray scattering (ASAXS) results described here report for the first time on the distribution of trivalent ions around DNA in solution and provide direct comparison of competition data to theoretical work. Simultaneous SAXS data monitor the state of the DNA. We find surprisingly good agreement between our data and Poisson-Boltzmann theories when ion size effects are included. For all conditions studied, this agreement is independent of ion type, ion shape, or DNA concentration. Measurement conditions span a large range of trivalent ion concentrations, from solutions containing no trivalent ions to trivalent concentrations at which the DNA begins to condense. From these data, we estimate the critical concentration of ions at the threshold of attraction.

BACKGROUND

Anomalous small-angle x-ray scattering

Solution small-angle x-ray scattering (SAXS), provides valuable experimental information about the conformation of (27) and interactions between (28) biomolecules. Anomalous small-angle x-ray scattering (ASAXS) exploits contrast variations to highlight the small-angle x-ray scattering from a single elemental component. All elements possess a unique set of characteristic energies, corresponding to electron binding energies, and can be individually targeted by tuning the energy of an x-ray beam until it exactly equals, or is resonant with, a specific electronic transition. This work focuses specifically on scattering from Rb^+ or $(Co(NH_3)_6)^{3+}$ ions through measurements carried out near the absorption edges of Rb or Co, respectively.

The ASAXS signal is obtained by measuring small-angle x-ray scattering profiles at two energies: one far below the resonant energy, and the second at a carefully selected energy just below the resonant energy, where the resonance affects sample scattering but not absorption (29). Proper normalization and subtraction of the signals removes energy-independent scattering; the remaining energy-dependent terms report on the spatial distribution of the resonant element. This technique has been used in past studies to investigate the distribution of ions around charged polyelectrolytes (30,31) and DNA (12,13).

The scattering amplitude from a two-component system, e.g., DNA and ions, is described by a sum of form factors:

$$A_s = f_{DNA}F_{DNA}(q) + f_{ion}F_{ion}(q). \quad (1)$$

In this equation, f_i is the scattering factor of the ith component and $F_i(q)$ is the Fourier transform of the spatial distribution of that component; the scattering vector $q = (4\pi/\lambda)\sin(\theta/2)$, where λ is the x-ray wavelength, and θ is the scattering angle. Since the scattering factors, f_i, are calculated relative to the bulk solution, contributions to the measured scattering arise solely from the DNA (which has a large electron density compared to the bulk solution) and the highly-concentrated ions that surround it. The measured scattering intensity is computed by multiplying the amplitude, A_s, and its complex conjugate:

$$I(q) = (f_{DNA}F_{DNA}(q) + f_{ion}F_{ion}(q))(f_{DNA}F_{DNA}(q) + f_{ion}F_{ion}(q))^*. \quad (2)$$

Near the resonant energy of the element/ion being investigated, the scattering factor, f_{ion}, contains a nonresonant term, f_o, in addition to two energy-dependent terms:

$$f_{ion}(E) = f_o + f'(E) + if''(E). \quad (3)$$

Here the real and imaginary parts of the scattering factor are given by f' and f'', respectively. The real part describes changes in the scattering intensity close to the resonant edge, while the imaginary part reflects changes in sample absorption.

To separate $I(q, E)$ into energy-dependent and energy-independent terms, it is useful to carry out the multiplication of Eq. 2. With the exception of f_{ion}, all quantities are real numbers:

$$I(E,q) = f_{DNA}^2F_{DNA}^2(q) + (f_{ion}(E) + f_{ion}^*(E))f_{DNA}F_{DNA}(q)F_{ion}(q) + f_{ion}(E)f_{ion}^*(E)F_{ion}^2(q). \quad (4)$$

Energy-independent terms vanish after subtraction of scattering profiles acquired at the two energies; the difference signal can be computed by inserting Eq. 3 into Eq. 4. We find

$$\Delta I(q) = \sim 2\Delta f'_{ion}f_{DNA}F_{ion}(q)F_{DNA}(q), \quad (5)$$

as an approximation for this difference, ignoring terms resulting from ion-ion scattering (12,13). Note, however, that measurement of the small term $(f'^2_{ion}F^2_{ion}(q))$ has been demonstrated by Ballauff and co-workers in a positively-charged polyelectrolyte system (31,32).

The scattering from any nonresonant ion species contributes another energy-independent term. However, it is small compared to the DNA scattering and does not contribute to the energy dependence of the scattering intensity.

DNA-DNA interactions, reported by the structure factor

Weak interactions between short DNA strands can be quantified by monitoring the small angle scattering at the lowest angles. The measured scattering intensity is the product of two terms: a so-called form factor that reflects the

scattering of each individual DNA, and a so-called structure factor that reflects interactions between adjacent DNAs. At low counterion concentrations, neighboring DNAs repel each other. In this case, the structure factor displays a strong peak, reflecting the short-range order of the self-avoiding DNA strands (28). As the counterion concentration increases, the DNAs no longer interact, and the measured scattering intensity for N DNAs equals N times the scattering of a single DNA, or N times the form factor. The onset of attractive forces between DNAs can be assayed by the appearance of an ''upturn'' at the lowest measured scattering angles. Importantly for this work, the structure factor that indicates attractive forces affects the scattering signal from the DNA only at the lowest angles accessible to the experiment, for $q < 0.05$ Å^{-1} (28). Previous experiments carried out by small-angle x-ray and light scattering suggest that short DNA strands stack end-to-end in the presence of moderate concentrations of divalent ions (33). This hypothesis was recently confirmed by studies of liquid crystal order in highly concentrated solutions of short DNAs (34). Although the nature of the trivalent ion-induced attraction reported here has yet to be explored, the changing structure factor appears to modify the scattering profiles only at $q <$ 0.05 Å^{-1}.

METHODS

ASAXS

ASAXS data were acquired at the C1 bend magnet station at the Cornell High Energy Synchrotron Source (CHESS). A schematic of the beamline is shown in Fig. 1. Tunable monochromatic x-rays were obtained from a double-bounce silicon monochromator. A polished silicon mirror acted as a low-bandpass filter, removing high-order harmonics from the beam. To increase the x-ray intensity through the sample, the beam was focused in the horizontal direction by the second monochromator crystal. No distortion resulted from the focusing. The beam size, ~3 mm wide and ~0.75 mm high, was set using slits. After passing through the sample, the scattered x-rays traveled through an evacuated flight tube. Near the exit of the flight tube, a motorized beamstop blocked the direct beam. An XFlash detector (Rontec, Carlisle, MA) was used to monitor the Compton scattering from the beamstop to obtain the intensity transmitted through the sample cell, allowing for proper intensity normalization of data. Scattering profiles were recorded using a homebuilt 1 K fiber-optic/CCD detector (35). The sample-to-detector distance was ~1 m.

Data were acquired near the K absorption energies, or edges, of both Rb (15.200 keV) and Co (7.709 keV). The energy resolution was ~8 eV and ~2 eV at the Rb and Co energies, respectively. To select the energies for the ASAXS measurements, transmission scans of a reference solution containing the ion of interest were examined. The energies were selected to maximize $\Delta f'$ while minimizing absorption and fluorescence. Nominal energies were 15.094 keV and 15.194 keV for Rb measurements and 7.514 keV and 7.714 keV for Co. The accessible q-range varied with energy: for the Rb energies, a q-range of 0.022–0.46 Å^{-1} was available; for the Co energies, the q-range was 0.018–0.22 Å^{-1}. Although the high-q cutoff was determined by energy, the low-q limit depended on the quality of beam, beam size, and positioning of the beamstop.

Sample cells were machined out of acrylic. Ultra-thin silicon nitride windows attached with glue minimized background absorption and scattering. Thinner cells were used at lower energies due to increased absorption. For measurements at the Co energy, the cell thickness was 0.68 mm, for the Rb cell, 2.6 mm was used.

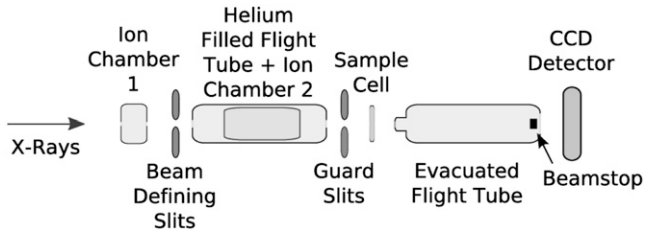

FIGURE 1 Schematic of the CHESS C-1 beamline, configured for ASAXS.

In addition to the correction for x-ray beam intensity, discussed above, all scattering profiles were corrected to account for small variations in DNA concentration by matching the amplitude of the scattering profiles in a q-range where the signal is strong, but unaffected by the structure factor. These concentrations were verified through absorbance measurements at 260 nm.

The ASAXS signals were determined by subtracting the resonant SAXS profile from the scattering data taken below the absorption edge. The number of ions bound to the DNA was computed by integrating the anomalous signal over the range $0.05 < q < 0.2$ Å^{-1}. This q-range is outside the region influenced by the structure factor.

Anomalous SAXS provides a relative measure of the number of the ions in the ion atmosphere surrounding the DNA as conditions change, not an absolute calibration. To convert the signal magnitude into a physically meaningful quantity, such as charge-compensated, a protocol for calibration must be employed. For measurements of Rb ions at the Rb energy, we prepared a ''reference'' DNA sample by dialysis into solution containing 100 mM RbCl. The integral of the measured anomalous signal from this sample was computed, and multiplied by a scale factor to equal the excess number (hence charge) of Rb^+ cations in the presence of DNA derived from Adaptive Poisson-Boltzmann Solver (APBS) computation. This is fewer than the number of phosphates on the DNA due to the known effect of anion depletion near the DNA, described extensively in Bai et al. (36). This scale factor was applied to all subsequent measurements of the anomalous signal from the Rb^+ ions.

To derive the excess number of $(Co(NH_3)_6)^{3+}$ ions present due to DNA, a different strategy must be applied to calibrate the integral of the anomalous signal. For these ions, a reference signal cannot be measured by ASAXS because the DNA aggregates in a solution containing only $(Co(NH_3)_6)^{3+}$ counterions. As an alternative, we used an equilibrium dialysis technique, inductively coupled plasma-atomic emission spectroscopy (ICP-AES), to measure the number of excess $(Co(NH_3)_6)^{3+}$ ions per phosphate for one of our samples (DNA in 0.2 mM $Co(NH_3)_6Cl_3$, 100 mM NaCl). The total charge due to excess $(Co(NH_3)_6)^{3+}$ ions is computed by multiplication of three with the number of phosphates present. The application of ICP-AES technique to ion counting is discussed extensively in the literature (26,36). The integral of the anomalous signal for this reference sample was multiplied by a scale factor to establish the conversion between the ASAXS signal and charge. This calibration factor was subsequently applied to the remaining anomalous signals from the $(Co(NH_3)_6)^{3+}$ ions. The ICP-AES measurements were made by the Cornell Nutrient Analysis Laboratories.

Data acquisition

Sixty-four independent SAXS profiles were used to compute a single ASAXS signal at the Co energy. The acquisition sequence involved switching between x-ray energies in the following sequence: nonresonant-energy; resonant-energy; resonant-energy; nonresonant-energy. To increase the signal/noise, this process was repeated 16 times. Additionally, two sets of 32 images measuring only the buffer solution were obtained in a similar

manner. The buffer measurements bracketed sample measurements to control for decay in x-ray beam intensity with time. Due to the higher quality of the signal (from reduction of the background scattering at high energy) for the Rb-energy data, one-half of the number of images sufficed. All images used 10 s x-ray exposures.

Anomalous signals at the Co energy were acquired by directly subtracting the resonant signal from the nonresonant signal of the DNA-containing sample. The higher signal/noise of data at the Rb energy allowed the use of DNA-buffer subtractions, permitting more straightforward corrections of systematic errors in the experimental setup.

Solutions

Lyophilized oligomers of 25 bp dsDNA, identical to those used in previous studies (13), were purchased from Integrated DNA Technology (Coralville, IA) and Operon Biotechnologies (Huntsville, AL). DNA was redissolved and annealed to ensure correct duplex formation. The samples were dialyzed until they reached equilibrium with the dialysis buffer. The equilibrium dialysis process controlled the free concentration of ions in the DNA solution, and allowed direct comparison to theories describing competition. The solutions were brought to a total volume of 40 μL for a [DNA] of 0.2 mM or 0.6 mM. All solutions contained 1 mM pH 7 Na-(3-(*n*-Morpholino)-propanesulfonic acid) (Na-MOPS). All samples contained 100 mM NaCl or RbCl, while the concentration of trivalent ions was varied from 0 to 1 mM. Separate solutions were made for all ICP and ASAXS measurements. The pH of the solutions was nominally 7, which was confirmed by measurement of recovered ASAXS samples. $Co(NH_3)_6Cl_3$, spermidine-3HCl, RbCl, NaCl, and Na-MOPS, were purchased from Sigma-Aldrich (St. Louis, MO).

Numerical calculations

The program APBS (37) was used to obtain the ''exact'' solution of the nonlinear Poisson-Boltzmann (NLPB) equation. In such a numerical approach, the geometry of the dsDNA is represented by the detailed atomic structure derived from its sequence, rather than cylindrical approximations as in most analytical treatments. Ions were assigned a common radius of 2, 3, or 6 Å to determine the ion-accessible surface along the dsDNA (38). Water was described as a dielectric medium with $\varepsilon = 78.54$. To obtain the excess number of counterions relative to their bulk concentration from the numerical NLPB solution, we integrated the number density of each type of ion over the whole box employed in the APBS computation. For sufficiently large boxes, the result was only weakly dependent on box size.

EXPERIMENTAL RESULTS

Scattering signals

ASAXS is a powerful tool for studying DNA and its associated counterions. As described in Methods, ASAXS data were obtained through careful subtraction of SAXS signals acquired at two closely-spaced energies. For example, differences in scattering profiles measured at 15.094 keV and 15.194 keV report on the distribution of Rb^+ ions. This subtraction removes large, energy-independent components of the scattering, leaving smaller, energy-dependent scattering from the resonant counterions around the DNA. The sensitivity of ASAXS to specific elements enables independent measurement of each ionic species. Information about the spatial distribution and number of ions bound is reported by the shape and amplitude of the ASAXS signal, respectively. In addition to the SAXS signals' importance in generating ASAXS data, the shape of the SAXS profiles reports on interactions between DNA molecules (28).

Fig. 2 illustrates how an ASAXS signal is derived from two SAXS profiles. The large panel shows SAXS data acquired at 15.094 keV and 15.194 keV, near the Rb edge, for DNA in a 100 mM RbCl, 1 mM Na-MOPS solution. The anomalous signal reporting on the Rb^+ ion distribution, Fig. 2, *inset*, is generated by subtracting these curves. The anomalous signal is generally an order-of-magnitude smaller than the SAXS data.

In this study, we use regular (nonresonant) SAXS to observe DNA-DNA interactions, while ASAXS is used to describe the counterion atmosphere that mediates these interactions. Signals measured at both the Rb and Co edges inform about the Rb^+ and $(Co(NH_3)_6)^{3+}$ ion distributions independently. We report on the SAXS and ASAXS signals for DNA in mixed solutions of $Co(NH_3)_6Cl_3$-RbCl, $Co(NH_3)_6Cl_3$-NaCl, and spermidineCl_3-RbCl.

Shape of counterion distributions

The shape of the ASAXS signals from Rb^+ and $(Co(NH_3)_6)^{3+}$ ions can be compared to assess the effect of ion valence on spatial distribution around DNA. In Fig. 3, Rb^+ (*solid*) and $(Co(NH_3)_6)^{3+}$ (*dash*) anomalous signals are shown for a DNA sample in a solution containing 100 mM RbCl, 0.5 mM $Co(NH_3)_6Cl_3$. The signals are matched at low-*q* to enable shape comparison. A signal from divalent Sr^{2+} ions (*dash-dot*), from a previous study, is also shown (13). As the valence of the ion increases from 1 to 3, there is a noticeable increase in scattering at high angle. It is generally accepted

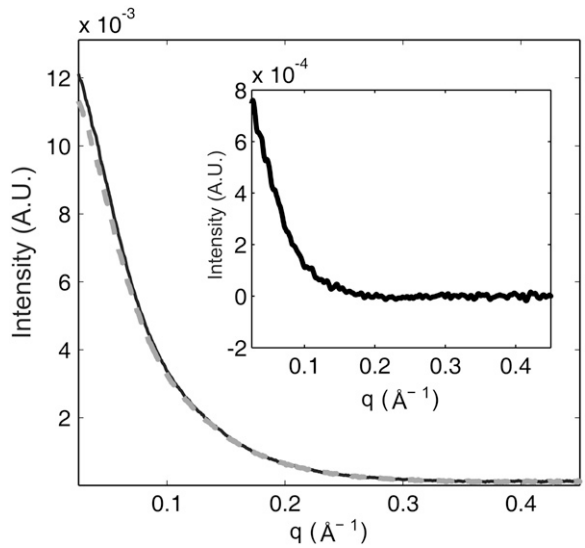

FIGURE 2 SAXS profiles of DNA acquired near the Rb edge. The solid line shows the profile acquired at the nonresonant energy, 15.094 keV. The dashed line shows scattering close to the edge, at 15.194 keV and reflects resonant effects. The anomalous signal, derived by subtraction of the resonant from nonresonant profile, is shown in the inset.

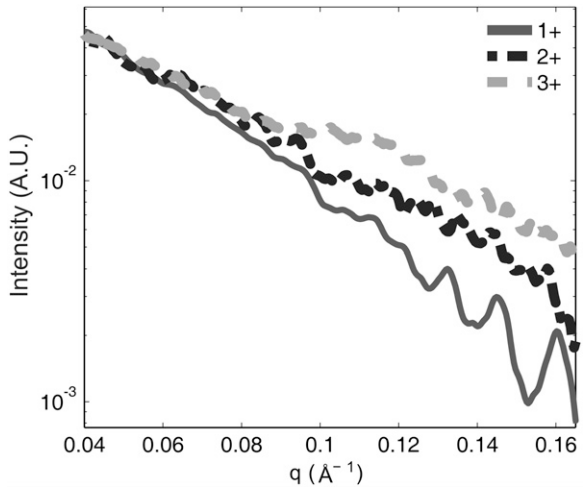

FIGURE 3 $(Co(NH_3)_6)^{3+}$ (*dash*), Sr^{2+} (*dot-dash*), and Rb^{+} (*solid*) ion ASAXS profiles, matched at low-*q*. The different shapes of the anomalous signals reflect differences in the spatial distribution of ions around the DNA. As the ion valence is increased, the weight of the scattering shifts to higher angle or *q*, indicating the tighter binding to the DNA of the more highly charged counterions.

that the scattering from a larger object falls off more rapidly with angle (or *q*) than the scattering from a smaller object. This angular dependence results from the more rapid onset of destructive interference due to the larger phase difference between x-rays scattered from more widely spaced electron pairs in larger, as opposed to smaller objects (39). In the case of ASAXS, the shape of the anomalous signal reflects the set of all vectors that have one end inside the DNA and the other end in the ion cloud. The lengths of these vectors are, on average, smaller if the ions are tightly localized to the DNA than if the ions are less well localized. Thus, an anomalous signal that persists to higher angle reflects a set of shorter vectors linking DNA and ions: more tightly bound counterions. This qualitative picture is supported by results described in a previous publication, where the NLPB form for mono and divalent counterions provided the decay length of the counterion distribution (13).

DNA-DNA interactions

The scattering profile of noninteracting DNAs is shown in Fig. 4 *a*. Increases in scattering at the lowest *q* relative to this curve indicate the onset of attractive forces between DNAs (28). Nonresonant SAXS profiles were examined as a function of increasing $(Co(NH_3)_6)^{3+}$ concentration (Fig. 4). At low $[(Co(NH_3)_6)^{3+}]$ of 0.2 mM in 100 mM monovalent ion and 0.2 mM DNA, the SAXS profiles are in good agreement with those obtained for noninteracting DNAs (Fig. 4 *a*). Changes in the low-*q* scattering were observed when the $(Co(NH_3)_6)^{3+}$ concentrations reached or exceeded 0.65 mM with a background of 100 mM monovalent ions. This change was reproducible; it was observed in samples measured at both the Rb and Co energies and during different experimental runs. To illustrate, the SAXS signals for solutions containing 0.2 mM, 0.65 mM, and 0.8 mM $[Co(NH_3)_6Cl_3]$, are shown at the nonresonant Rb energy (Fig. 4 *b*), and for $[Co(NH_3)_6Cl_3] = 0.2$ mM and 0.8 mM at the nonresonant Co energy (Fig. 4 *c*). An increase in scatter at low-*q* is measured for the 0.8 mM $Co(NH_3)_6Cl_3$ sample at both energies. More $Co(NH_3)_6Cl_3$ concentrations were probed at the Rb energy; these more finely spaced points show the onset of attraction at $[Co(NH_3)_6Cl_3] = 0.65$ mM. Intriguingly, SAXS signals at $[Co(NH_3)_6Cl_3] > 1.0$ mM revert to the noninteracting shape. This effect most likely results from aggregation and precipitation of some of the DNA at these higher free $(Co(NH_3)_6)^{3+}$ concentrations; the precipitated DNA is not detectable by solution SAXS.

To investigate the effect of counterion size and geometry on ion binding and DNA-DNA interactions, an identical series of measurements was carried out substituting the long, linear trivalent spermidine^{3+} ions for $(Co(NH_3)_6)^{3+}$. The (higher concentration) spermidine^{3+} samples displayed a similar, though somewhat weaker, increase in the SAXS profile at low-*q*.

In summary, SAXS data were acquired from DNA in solutions containing increasing numbers of trivalent ions. At the lowest trivalent ion concentration, scattering profiles indicate that the DNAs are noninteracting; however, attraction is evident as the number of multivalent ions increases. We now discuss ASAXS data from the same samples, which provides information about the composition of the ion atmosphere.

ASAXS

ASAXS was used to determine the fractional contribution of each cationic species to the ion atmosphere around DNA. When multivalent ions are introduced, they compete favorably with monovalent ions in the charge neutralization of DNA due to the entropic gain of binding one +3 ion compared to three +1 ions. ASAXS provides a direct measurement of this competition; the association or dissociation of ions is reflected by an increase or decrease in the anomalous signal. These changes in amplitude can be quantified by integrating the anomalous signals at each energy. As described in Methods, each anomalous signal is scaled to reflect the DNA charge, compensated by each ion type. Fig. 5 shows the integrals of the ASAXS signals at the Rb and Co energies and the comparison to the predictions of the Poisson-Boltzmann equation.

Rb energy

The upper points of Fig. 5 show the integrals of the ASAXS signals at the Rb energy, yielding the relative number of Rb^{+} ions bound to the DNA, in competition with $(Co(NH_3)_6)^{3+}$ (*circles*) and spermidine^{3+} (*squares*). In both experiments

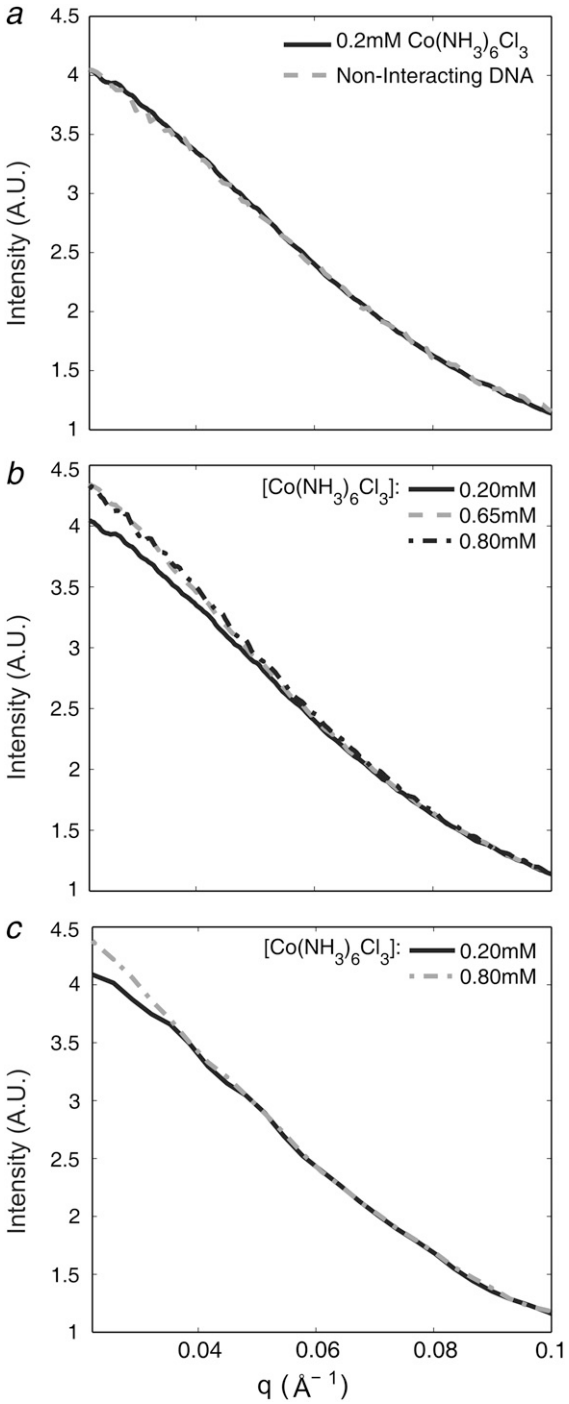

FIGURE 4 Inter-DNA attraction assessed from nonresonant scattering profiles. (*a*) The dashed curve shows scattering of noninteracting DNA (28). The solid curve shows a SAXS profile of DNA in 100 mM RbCl and 0.2 mM $Co(NH_3)_6Cl_3$. The similarity of these profiles suggests no interaction between DNAs at this low concentration of $(Co(NH_3)_6)^{3+}$. However, when more $(Co(NH_3)_6)^{3+}$ is added (*b* and *c*), an ''upturn'' in the SAXS profiles appears at $q < 0.04$ Å^{-1}, indicating weak attraction between DNAs. (*b*) SAXS profiles acquired at the nonresonant energy associated with the Rb edge in solutions containing 0.2 mM (*solid*), 0.65 mM (*dash*), or 0.8 mM (*dot-dash*) $Co(NH_3)_6Cl_3$, monovalent ion concentration kept at 100 mM RbCl. Data taken at 0.35 mM and 0.5 mM $Co(NH_3)_6Cl_3$ coincide with the 0.2 mM scattering profile within error (not shown). (*c*) SAXS profiles acquired at the nonresonant energy associated with the Co edge in solutions containing 0.2 mM (*solid*) and 0.8 mM (*dot-dash*) $Co(NH_3)_6Cl_3$, monovalent at 100 mM NaCl.

the Rb signals show a marked decrease as the concentration of the respective trivalent ion increases. As anticipated, the trivalent ions compete very effectively against the monovalent Rb^+. Surprisingly, the data for these two very different trivalent ions agree within error; the ions compete in an apparently purely electrostatic manner. The broken lines shows the prediction of numerical solutions of the Poisson-Boltzmann equation derived from APBS for several ion sizes. A 3 Å ion radius represents a reasonable lower bound for ion size; the precision of the data do not warrant a more precise estimate.

Co energy

We applied a similar analysis to derive the number of $(Co(NH_3)_6)^{3+}$ ions bound to the DNA for measurements acquired at the Co edge. Because of the inherent difficulties in measuring at this low x-ray energy (<8 keV), the samples were modified slightly to reduce absorption: Na^+ was used instead of Rb^+ due to its reduced electron density. To control for differences between Na^+ and Rb^+ ions, the Co-ASAXS signal from a $(Co(NH_3)_6)^{3+}$-Rb^+ competition series was also measured, though at a higher DNA concentration of 0.6 mM. As an additional control for DNA concentration variations, $(Co(NH_3)_6)^{3+}$-Na^+ competition was also measured at 0.6 mM [DNA].

All ASAXS signals were integrated and the fraction of DNA charge compensated was computed by scaling the integrated signal to ICP data, as described in Methods. These data are plotted in Fig. 5 (*lower points*). The good agreement between all data indicates that the measured $(Co(NH_3)_6)^{3+}$ competition is independent of DNA concentration and monovalent ion identity. Furthermore, anomalous signals are well described by the same numerical solutions of the Poisson-Boltzmann equation used for the Rb-energy ASAXS data. The solution is shown as a dashed line in Fig. 5; again, surprisingly good agreement is achieved.

At $[Co(NH_3)_6Cl_3] \geq 1$ mM, the system becomes irreproducible and difficult to control, varying with both time and x-ray exposure. Above 2 mM $[Co(NH_3)_6Cl_3]$, visible precipitates were present in the solution and precluded reliable solution scattering studies.

Finally, it is interesting to note how little $(Co(NH_3)_6)^{3+}$ is needed to compete with the Rb^+ atmosphere. At 0.2 mM $Co(NH_3)_6Cl_3$, the $(Co(NH_3)_6)^{3+}$ contributes 0.6% of the charge fraction in the bulk solution while $(Co(NH_3)_6)^{3+}$ ions compensate 21% of the DNA charge. Total DNA charge compensation is observed at all $[Co(NH_3)_6Cl_3]$ as predicted within the Poisson-Boltzmann framework.

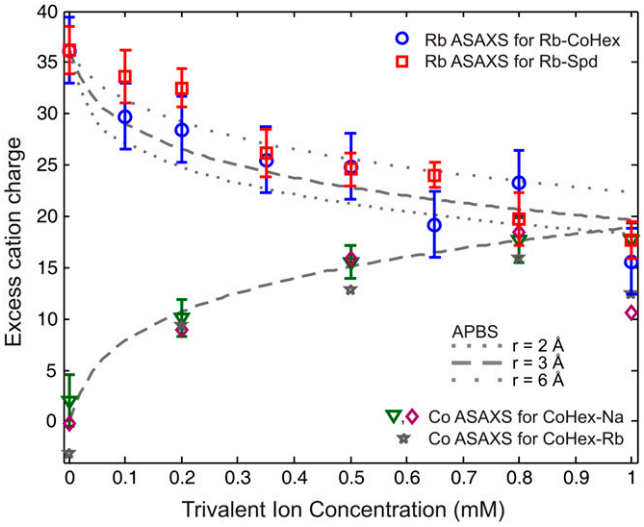

FIGURE 5 Comparison of counterion competition data with the numerical solution of the PB equation. (*Upper-half*) DNA charge compensated by Rb^+ ions in competition with $(Co(NH_3)_6)^{3+}$ (*circles*) and spermidine^{3+} (*squares*) in 100 mM RbCl, 0.2 mM [DNA]. (*Lower-half*) DNA charge compensated by $(Co(NH_3)_6)^{3+}$ ions in competition with 100 mM NaCl at 0.2 mM [DNA] (*triangles*) and in competition with 100 mM NaCl (*diamonds*) or RbCl (*stars*) at 0.6 mM [DNA]. Data without error bars have errors smaller than symbol size. The dashed lines represent APBS computations for DNA surrounded by ions with different radii. A 2 Å ion radius underestimates the fraction of monovalent ions in the atmosphere. The data are consistent with ion radii of 3 Å or greater with an upper bound of 6 Å.

DISCUSSION

This study was designed to explore the connection between the ion atmosphere around DNA and inter-DNA interactions. Numerous theories predict that correlations should increase the number of trivalent ions bound to DNA (5,7). These correlations should lead to inter-DNA attraction, observable by SAXS, as the trivalent ions compensated the DNA charge.

Surprisingly, we observed agreement with atomic-scale models based on the Poisson-Boltzmann equation for all measurements below the precipitation regime. For the lowest trivalent ion concentrations ≤0.5 mM, this agreement is not unexpected. Although continuum theories are expected to break down due to counterion correlations, a critical concentration of trivalent ions must first be reached. The noninteraction of DNAs at these low concentrations suggests that this regime was not yet achieved.

The most intriguing results were found at trivalent ion concentrations between 0.65 mM and 0.8 mM. At these concentrations, inter-DNA attractions, albeit weak, were observed (Fig. 4). Despite this evidence for attraction, the number of ions around the DNA continued to agree well with the Poisson-Boltzmann predictions. This result is counter-intuitive, as correlations should be seen before attraction. Attempts to measure at higher $[Co(NH_3)_6Cl_3]$ were unsuccessful, as the system becomes inhomogeneous when precipitation occurs at free $[Co(NH_3)_6Cl_3] \geq 1.0$ mM.

The simplest explanation for the agreement with Poisson-Boltzmann is that the correlation effects are below our detection limits; our current measurements have an accuracy of ~10%. Any increase in trivalent binding of this order or smaller, would be undetectable. This provides an estimated upper limit of counterion correlation effects on the binding of trivalent ions.

From the observed onset of attraction and the magnitude of the anomalous signal at the Co edge (Fig. 5), we can obtain an estimate of the number of ions required for DNA-DNA interaction. At 0.5 mM $[Co(NH_3)_6Cl_3]$, no attraction is observed. Under these conditions, there are five trivalent ions per 25 bp DNA, equivalent to a linear density of ~1 $(Co(NH_3)_6)^{3+}$ ion per 5 bp (17 Å). As the concentration of $Co(NH_3)_6Cl_3$ increases to 0.8 mM, attraction is observed. Under these conditions, the anomalous signal reports ~6 ions per DNA, equivalent to one $(Co(NH_3)_6)^{3+}$ ion per 4.2 bp (14 Å). Since the attraction is first measured at 0.65 mM (from Rb-energy data), the actual number of ions needed for attraction is slightly less than 6 per 25 bp DNA. A difference of ~1 ion per DNA is sufficient to cause a transition of the DNA from a noninteracting to interacting regime. This does not imply that the transition is discrete; due to the small number of trivalent ions involved, the experiment is highly sensitive to changes, even to the addition of one ion per DNA. Direct measurement of correlations between DNA counterions may be possible using the ASAXS method demonstrated by Ballauff and co-workers in a positively-charged polyelectrolyte system (31,32). This approach necessitates SAXS measurements at numerous closely-spaced x-ray energies and is potentially challenging because of signal/noise considerations in DNA SAXS experiments. We are currently exploring this approach to extract the ion-ion scattering term from this system.

A second notable result comes from the agreement in the competition data of spermidine or $(Co(NH_3)_6)^{3+}$ with Rb^+ shown in Fig. 5. Some studies have reported similarities in trivalent binding constants over a large range of concentrations (26), while others predict strong differences due to size, shape, or charge density considerations (22,23). We observe that agreement between the data and Poisson-Boltzmann theory is found only if finite ion sizes are included. Here, the data can be relatively well represented by ions assigned a 3 Å radius, a reasonable value for Rb^+, Na^+, and $(Co(NH_3)_6)^{3+}$ (13,38). Spermidine^{3+}, however, is much larger; its longest dimension is on the order of 10 Å. This apparent inconsistency can be resolved by considering how size affects ion binding. Ion size modifies the distance of closest approach of the ion (8,13); steric interactions prohibit the ion from reaching its electrostatic free energy minimum. In effect, the DNA diameter appears larger. Spermidine^{3+} is quite unlikely to have the same distance of closest approach as $(Co(NH_3)_6)^{3+}$ if its linear axis lies perpendicular to the DNA linear axis. However, if the linear axes are aligned, a distance of closest approach of 3 Å is not unreasonable.

CONCLUSION

Using ASAXS, we measured the distribution of trivalent ions in competition with monovalent ions for charge compensation of DNA. In addition, we measured the inter-DNA interactions resulting from the localization of trivalent ions to the DNA. Quantitative agreement between competition and models of the size-corrected Poisson Boltzmann formalism was found over a surprisingly large range, up to and including the regime where DNA-DNA attraction was observed. This result is valid for both monovalent and trivalent ions and is, for conditions tested, independent of ion type, geometry, or linear size. By careful coordination of all measurements, we estimate the distance between ions at the onset of attraction, perhaps analogous to a correlation length, to be one trivalent ion for 14 Å along the DNA chain, corresponding to 4.2 basepairs.

We thank Ken D. Finkelstein for experimental assistance and Tom Lograsso for the amorphous metal beamstop material.

This research is funded by the National Science Foundation through grant No. MCB-0347220, and The Nanobiotechnology Center at Cornell. Additional support was provided by the National Institutes of Health through grant No. P01-GM066275. CHESS is supported by the National Science Foundation and the National Institutes of Health/National Institute of General Medical Sciences under grant No. DMR-9713424. The Cornell NanoScale Science & Technology Facility is supported by the National Science Foundation, Cornell University, and industrial affiliates.

REFERENCES

1. Manning, G. S. 1969. Limiting laws and counterion condensation in polyelectrolyte solutions. 1. Colligative properties. *J. Chem. Phys.* 51: 924.
2. Lebret, M., and B. H. Zimm. 1984. Distribution of counterions around a cylindrical polyelectrolyte and Manning condensation theory. *Biopolymers.* 23:287–312.
3. Gueron, M., and G. Weisbuch. 1980. Poly-electrolyte theory. 1. Counterion accumulation, site-binding, and their insensitivity to polyelectrolyte shape in solutions containing finite salt concentrations. *Biopolymers.* 19:353–382.
4. Raspaud, E., D. Durand, and F. Livolant. 2005. Interhelical spacing in liquid crystalline spermine and spermidine-DNA precipitates. *Biophys. J.* 88:392–403.
5. Nguyen, T. T., I. Rouzina, and B. I. Shklovskii. 2000. Reentrant condensation of DNA induced by multivalent counterions. *J. Chem. Phys.* 112:2562–2568.
6. Yang, J., and D. C. Rau. 2005. Incomplete ion dissociation underlies the weakened attraction between DNA helices at high spermidine concentrations. *Biophys. J.* 89:1932–1940.
7. Solis, F. J., and M. O. de la Cruz. 2001. Flexible linear polyelectrolytes in multivalent salt solutions: solubility conditions. *Eur. Phys. J. E.* 4: 143–152.
8. Rouzina, I., and V. A. Bloomfield. 1997. Competitive electrostatic binding of charged ligands to polyelectrolytes: practical approach using the non-linear Poisson-Boltzmann equation. *Biophys. Chem.* 64:139–155.
9. Gueron, M., J. P. Demaret, and M. Filoche. 2000. A unified theory of the B-Z transition of DNA in high and low concentrations of multivalent ions. *Biophys. J.* 78:1070–1083.
10. Bloomfield, V. A. 1996. DNA condensation. *Curr. Opin. Struct. Biol.* 6:334–341.
11. Anderson, C. F., and M. T. Record. 1990. Ion distributions around DNA and other cylindrical polyions—theoretical descriptions and physical implications. *Annu. Rev. Biophys. Biophys. Chem.* 19:423–465.
12. Das, R., T. T. Mills, L. W. Kwok, G. S. Maskel, I. S. Millett, S. Doniach, K. D. Finkelstein, D. Herschlag, and L. Pollack. 2003. Counterion distribution around DNA probed by solution x-ray scattering. *Phys. Rev. Lett.* 90:188103.
13. Andresen, K., R. Das, H. Y. Park, H. Smith, L. W. Kwok, J. S. Lamb, E. J. Kirkland, D. Herschlag, K. D. Finkelstein, and L. Pollack. 2004. Spatial distribution of competing ions around DNA in solution. *Phys. Rev. Lett.* 93:248103.
14. Guilleaume, B., J. Blaul, M. Wittemann, M. Rehahn, and M. Ballauff. 2000. Investigations of rodlike polyelectrolytes in solution by small-angle x-ray scattering. *J. Phys. Cond. Matt.* 12:A245–A251.
15. Hecht, J., B. Honig, Y.-K. Shin, and W. Hubbell. 1995. Electrostatic potentials near the surface of DNA: comparing theory and experiment. *J. Phys. Chem.* 99:7782–7786.
16. Pack, G. R., L. Wong, and G. Lamm. 1999. Divalent cations and the electrostatic potential around DNA: Monte Carlo and Poisson-Boltzmann calculations. *Biopolymers.* 49:575–590.
17. Grosberg, A. Y., T. T. Nguyen, and B. I. Shklovskii. 2002. Colloquium: The physics of charge inversion in chemical and biological systems. *Rev. Mod. Phys.* 74:329–345.
18. Ha, B. Y., and A. J. Liu. 1997. Counterion-mediated attraction between two like-charged rods. *Phys. Rev. Lett.* 79:1289–1292.
19. Pelta, J., F. Livolant, and J. L. Sikorav. 1996. DNA aggregation induced by polyamines and cobalt-hexamine. *J. Biol. Chem.* 271:5656–5662.
20. Raspaud, E., M. O. de la Cruz, J. L. Sikorav, and F. Livolant. 1998. Precipitation of DNA by polyamines: a polyelectrolyte behavior. *Biophys. J.* 74:381–393.
21. Angelini, T. E., H. Liang, W. Wriggers, and G. C. L. Wong. 2003. Like-charge attraction between polyelectrolytes induced by counterion charge density waves. *Proc. Natl. Acad. Sci. USA.* 100:8634–8637.
22. Burak, Y., G. Ariel, and D. Andelman. 2003. Onset of DNA aggregation in presence of monovalent and multivalent counterions. *Biophys. J.* 85:2100–2110.
23. Burak, Y., G. Ariel, and D. Andelman. 2004. Competition between condensation of monovalent and multivalent ions in DNA aggregation. *Curr. Opin. Colloid Interface Sci.* 9:53–58.
24. Ma, C. L., and V. A. Bloomfield. 1995. Gel-electrophoresis measurement of counterion condensation on DNA. *Biopolymers.* 35:211–216.
25. Braunlin, W. H., C. F. Anderson, and M. T. Record. 1986. Na-23-NMR investigations of counterion exchange-reactions of helical DNA. *Biopolymers.* 25:205–214.
26. Plum, G. E., and V. A. Bloomfield. 1988. Equilibrium dialysis study of binding of hexamine cobalt^{III} to DNA. *Biopolymers.* 27:1045–1051.
27. Doniach, S. 2001. Changes in biomolecular conformation seen by small angle x-ray scattering. *Chem. Rev.* 101:1763–1778.
28. Qiu, X. Y., L. W. Kwok, H. Y. Park, J. S. Lamb, K. Andresen, and L. Pollack. 2006. Measuring inter-DNA potentials in solution. *Phys. Rev. Lett.* 96:138101.
29. Naudon, A. 1995. Modern Aspects of Small-Angle Scattering. Kluwer Academic Publishers, Dordrecht; Boston.
30. Sabbagh, I., M. Delsanti, and P. Lesieur. 1990. Ionic distribution and polymer conformation, near phase separation, in sodium polyacrylate/divalent cations mixtures: small angle x-ray and neutron scattering. *Annu. Rev. Biophys. Biophys. Chem.* 19:301–332.
31. Ballauff, M., and A. Jusufi. 2006. Anomalous small-angle x-ray scattering: analyzing correlations and fluctuations in polyelectrolytes. *Colloid Polym. Sci.* 284:1303–1311.
32. Patel, M., S. Rosenfeldt, M. Ballauff, N. Dingenouts, D. Pontoni, and T. Narayanan. 2004. Analysis of the correlation of counterions to rod-like macroions by anomalous small-angle x-ray scattering. *Phys. Chem. Chem. Phys.* 6:2962–2967.

33. Qiu, X. Y., K. Andresen, L. W. Kwok, J. S. Lamb, H. Y. Park, and L. Pollack. 2007. Inter-DNA attraction mediated by divalent counterions. *Phys. Rev. Lett.* 99:038104.

34. Nakata, M., G. Zanchetta, B. Chapman, C. Jones, J. Cross, R. Pindak, T. Bellini, and N. Clark. 2007. End-to-end stacking and liquid crystal condensation of 6 to 20 base pair DNA duplexes. *Science*. 318:1276–1279.

35. Tate, M. W., E. F. Eikenberry, S. L. Barna, M. E. Wall, J. L. Lowrance, and S. M. Gruner. 1995. A large-format high-resolution area x-ray-detector based on a fiber-optically bonded charge-coupled-device (CCD). *J. Appl. Cryst.* 28:196–205.

36. Bai, Y., M. Greenfeld, K. J. Travers, V. B. Chu, J. Lipfert, S. Doniach, and D. Herschlag. 2007. Quantitative and comprehensive decomposition of the ion atmosphere around nucleic acids. *J. Am. Chem. Soc.* 129: 14981–14988.

37. Baker, N. A., D. Sept, S. Joseph, M. J. Holst, and J. A. McCammon. 2001. Electrostatics of nanosystems: application to microtubules and the ribosome. *Proc. Natl. Acad. Sci. USA*. 98:10037–10041.

38. Deng, H., and V. A. Bloomfield. 1999. Structural effects of cobalt-amine compounds on DNA condensation. *Biophys. J.* 77:1556–1561.

39. Glatter, O., and O. Kratky. 1982. Small Angle X-Ray Scattering. Academic Press, London.